JOURNAL OF APPLIED PHYSICS 115, 223302 (2014)

Heating mode transition in a hybrid direct current/dual-frequency capacitively coupled CF_4 discharge

Quan-Zhi Zhang,[1,2,a)] You-Nian Wang,[1] and Annemie Bogaerts[2]
[1]School of Physics and Optoelectronic Technology, Dalian University of Technology, Dalian 116024, China
[2]Department of Chemistry, University of Antwerp, Campus Drie Eiken, Universiteitsplein 1, BE-2610 Wilrijk-Antwerp, Belgium

(Received 27 March 2014; accepted 28 May 2014; published online 10 June 2014)

Computer simulations based on the particle-in-cell/Monte Carlo collision method are performed to study the plasma characteristics and especially the transition in electron heating mechanisms in a hybrid direct current (dc)/dual-frequency (DF) capacitively coupled CF_4 discharge. When applying a superposed dc voltage, the plasma density first increases, then decreases, and finally increases again, which is in good agreement with experiments. This trend can be explained by the transition between the four main heating modes, i.e., DF coupling, dc and DF coupling, dc source dominant heating, and secondary electron dominant heating. © *2014 AIP Publishing LLC*. [http://dx.doi.org/10.1063/1.4882297]

I. INTRODUCTION

Dual-frequency (DF) capacitively coupled radio frequency (CCRF) discharges are widely used for industrial applications, such as etching and deposition processes.[1,2] In many of these applications, reactive electronegative gases such as CF_4[1] are required.

The concept of a traditional DF CCRF discharge[3–8] is driving the plasma with two substantially different frequencies to achieve separate control of ion flux and energy. The low frequency (LF) component usually operates with large voltage amplitude to control the ion energy and angular distributions, whereas the high frequency (HF) component with small voltage amplitude is typically used to determine the plasma density and ion flux. Lai *et al.*[9] and Yamaguchi *et al.*[10,11] have experimentally shown that the plasma density and the etch rate can be increased by introducing an extra negative direct current (dc) potential to the RF discharge. Yamaguchi *et al.* also pointed out that the superposed negative dc bias can significantly improve the selectivity of the etching of SiOCH over SiC in a DF CF_4 discharge. Therefore, this kind of hybrid dc/RF plasma source has received increased attention recently in both industrial and academic fields.[11–20]

When a negative dc voltage is applied to the electrode, the sheath structure is determined by the superposition of a dc sheath and an RF sheath.[12,13] Under the effect of the large potential drop in the dc/RF sheath, ions are attracted to bombard the dc electrode continuously, and abundant secondary electrons are thus emitted and accelerated toward the plasma. It is generally believed that these high energy secondary electrons play an important role in determining the beneficial characteristics in dc/RF plasmas. Kawamura *et al.*[12,13] pointed out by means of one-dimensional (1D) and two-dimensional (2D) particle-in-cell/Monte Carlo collision (PIC/MCC) simulations that the mean secondary electron energy increases upon the introducing of an extra dc source to the discharge, which results in an overall increase in the discharge efficiency, i.e., the effective energy loss for the generation of one electron-ion pair decreases, and consequently the plasma density increases. At somewhat higher pressures, Jiang *et al.*[14] found similar results with lower secondary electron emission coefficients, again by using 1D PIC/MCC simulations. They reported that a one-side α–γ discharge mode transition occurred with increasing dc voltage near the dc electrode. By performing test particle Monte Carlo simulations, Denpoh and Ventzek[15,16] showed that adding the dc source results in a small peak, which corresponds to the maximum energy of high energy secondary electrons, appearing in the tail of the electron energy distribution function (EEDF). Xu *et al.*[17] later confirmed their result experimentally. Furthermore, Wang *et al.*[18] and Diomede *et al.*[20] studied the detailed dependency relationship of the peak of maximum electron energy (in the EEDF) on the source voltage in different discharge configurations, by using a 2D hybrid plasma equipment model and a PIC-MCC/fluid hybrid model, respectively. They both pointed out that these highly directional electrons may alleviate the differential charging of the bottom and sidewalls in case of insulating films.

However, although a lot of effort has been put in the study of dc superposed CCRF discharges and in the effect of secondary electrons in hybrid dc/RF discharges, the dependence of the secondary electron behavior on the dc bias and the effect of other inherent factors, such as the coupling of dc and RF voltage, in a DF electronegative gas discharge are still unclear. In this paper, we pay particular attention to the heating mechanisms at different dc voltages in hybrid dc/DF CCRF CF_4 discharges by means of self-consistent PIC/MCC simulations. It will be shown that when the dc voltage is comparable to the LF source amplitude, the coupling of dc and DF voltage will become the main heating mechanism, and this gives rise to an increase in the plasma density. When the dc voltage is slightly larger than the LF source amplitude, the dc bias will dominate the discharge and this results in a compressed bulk region and hence a decrease of the plasma density. However, when the dc voltage becomes high enough, the high energy secondary electrons originating

a)qzzhangdlut@gmail.com

from the dc electrode contribute most to the ionization, which gives rise to an increase of the plasma density again. This calculated trend of plasma density with rising dc voltage has been compared with experimental data operated with similar parameters in a commercially available dual-frequency CCP reactor, and good agreement has been achieved. This paper is organized as follows: in Sec. II, the details of the simulations are outlined. Results are presented in Sec. III, where we show the variation of plasma density with rising dc voltage, and discuss the transitions between different heating modes. A short conclusion is drawn in Sec. IV.

II. PIC/MCC COUPLED SIMULATIONS

We employ here a 1D3V (one dimensional in space and three-dimensional in velocity) electrostatic PIC method coupled with a MCC model[21–23] to simulate a symmetric discharge with two parallel plate electrodes separated by a gap of L = 3 cm and filled with pure CF_4 gas at 70 mTorr. One electrode at x = 0 is driven by a negative dc source and a LF source and the other electrode at x = L is powered by an HF source. The driving voltage waveform of the LF and HF source is $V_{lf}\sin(2\pi f_{lf} t)$ and $V_{hf}\sin(2\pi f_{hf} t)$, where f_{lf} and f_{hf} correspond to the LF of 2 MHz and HF of 60 MHz, respectively, and V_{lf}, V_{hf} are their voltage amplitudes. In the simulation, V_{lf} is kept at 250 V, and V_{hf} is set at 210 V.

In experimental systems with a blocking capacitor in the external circuit, the dc component of the current cannot go through the capacitor. When introducing a dc source, the corresponding dc current can only flow between the dc electrode and the grounded chamber wall. However, including the chamber wall is beyond the scope of our 1D model. Hence, if a blocking capacitor is still used in our 1D model, the charges will accumulate on the capacitor, and a self-bias will be generated to compensate for the applied dc voltage, until the net dc bias between the two electrodes becomes zero. Therefore, in this work, we do not consider any blocking capacitors, and the RF and dc voltage source are applied to the electrodes directly, as is widely done in many previous simulations.[12–16,20] By means of this method, the effect of the additional dc voltage can be studied with a 1D model.

Four types of charged species, i.e., CF_3^+, CF_3^-, F^- ions, and the electrons are traced in the code. In the Monte Carlo collision part, we take into account the same collision processes as in Ref. 24. Both the ion-induced and electron-induced secondary-electron emission are considered. The initial velocities of these secondary electrons are calculated from the Maxwellian distribution at an average electron temperature of 3 eV. The secondary electrons are emitted toward the plasma in an isotropic way.

An explicit scheme is used in all simulations. The space step dx is fixed to 3.0×10^{-5} m, and the time steps dt_e for electrons and dt_i for ions are fixed to 1.0×10^{-11} s and 1.6×10^{-10} s, respectively. When the discharge reaches equilibrium, the values of dx/λ and $\omega_{pe} \cdot dt$ are $0.60 \sim 0.78$ and $0.10 \sim 0.14$, respectively, where λ is the Debye length and ω_{pe} is the plasma frequency. We use at least 200 super-particles per cell for all the simulations, which satisfies the convergence conditions as discussed by Turner,[25] and we typically run the code for over 600 LF cycles to reach convergence. The initial ion and electron temperatures are set as 0.026 eV and 3 eV, respectively. All the presented results in this paper are calculated after the plasma reaches equilibrium.

III. RESULTS AND DISCUSSIONS

A. Effect of dc bias on the plasma density

In Figure 1, we show the calculated time-averaged density profiles of the various plasma species in a DF discharge without additional dc bias. The ion-induced and electron-induced secondary-electron emission coefficients, γ_i and γ_e, are taken as 0.3 and 0.2,[26] respectively. As can be seen, all the species have a symmetric and concave density profile and the electron density is much higher than the negative ion density, i.e., the discharge is mainly electropositive at the conditions under study. This is in agreement with other published results, which were also obtained at low pressure.[27,28]

Figure 2 shows the calculated time-averaged electron density profiles for various dc voltages, in comparison to experimental data, obtained from Ref. 11. These experiments were carried out using a DF-CCRF reactor in which the HF (60 MHz) source and a negative dc source were simultaneously applied to one electrode, and the LF (13.56 MHz) source was applied at the other electrode. The distance between the electrodes is fixed at 35 mm. A mixture of Ar, N_2 and $c-C_4F_8$ gases of 40 mTorr was introduced. Note that in our simulations, the LF source and a negative dc source were applied to one electrode, whereas the other electrode was powered by the HF source. Hence, this is not exactly the same as in the experiments. However, due to the symmetry of the 1D model, it makes no difference to which electrode the power source is applied; and since the discharge parameters in the experiments are very similar with our simulations, the qualitative comparison shown in Figure 2 is thus reasonable.

Note that the experimental plasma densities were plotted on a relative axial position normalized by the electrode gap distance. In the simulation results (Figure 2(a)), the addition of a dc voltage results in a shift of the plasma bulk away

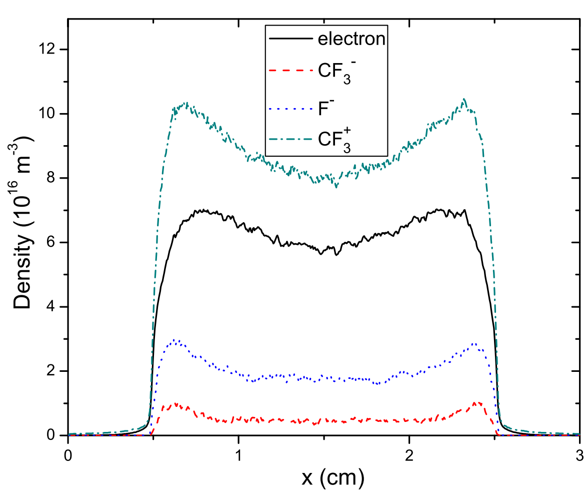

FIG. 1. Calculated time-averaged density profiles of the various plasma species in a DF discharge operated at 70 mTorr, without dc voltage.

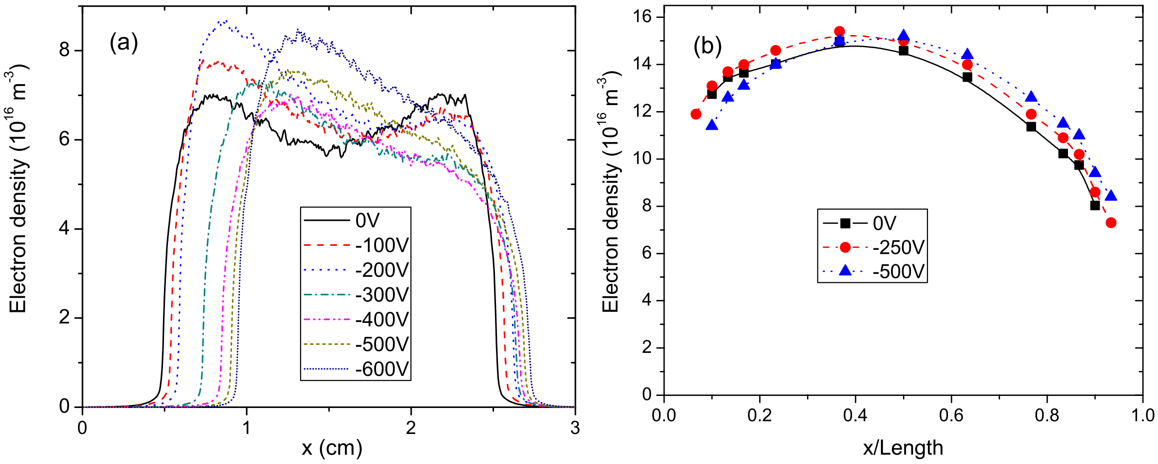

FIG. 2. Time-averaged calculated (a) and measured[11] (b) electron density profiles for various dc voltages.

from the dc-powered electrode, and at the same time the plasma bulk is largely compressed and the electron density profile changes from concave to parabolic around -300 V dc bias. A minor shift of the plasma bulk away from the dc-powered electrode and a minor change in profile can also be deduced from the experimental density profiles (Figure 2(b)), but the effect is not so pronounced. It should be noted that the pressure used in the simulation (70 mTorr) is somewhat higher than in the experiment (40 mTorr), which makes that the local motion of electrons becomes more dominant. Indeed, at higher pressure, the velocity of the electrons is damped dramatically by the frequent collisions with neutral species. Thus, the calculated density profiles are somewhat different from the experimental results, and the peak density appears where most ionization occurs (see further in Sec. III B below). The relatively larger shift of the plasma bulk in the simulations is probably due to the limitation of the 1D model in which the geometrical factor cannot be considered. The geometrical asymmetry in a CCP reactor may cause a small dc self-bias, which can compensate to some degree for the applied dc bias.[13] Finally, the calculated electron density values are a factor of 2 lower than the measured values, which we consider still as a reasonable agreement, in view of the complexity of the model and the differences in the discharge parameters between simulation and experiment.

The calculated peak values of the electron density are plotted as a function of dc bias in Figure 3, together with the measured values, adopted from Ref. 11. The peak value of the calculated electron density first increases when adding a small dc bias (up to -200 V), then it decreases for slightly higher negative dc bias values (up to -400 V), and finally it increases again at high enough negative dc voltages (between -400 and -600 V). This behavior is in qualitative agreement with the experimental results, although the trend is a bit less pronounced for the initial rise and subsequent drop. In Sec. III B, we will try to elucidate the underlying physics responsible for this trend.

B. Heating mode transitions

Figure 4(a) shows the calculated time-averaged ionization rate profiles for various dc voltages. The peak in the ionization rate near the HF powered electrode (at $x = 3$ cm) decreases monotonically with rising dc voltage, and hence the profile shifts from a double peak distribution to a single peak. This explains the change in electron density profiles shown in Figure 2. The spatially integrated ionization rate is plotted vs. dc voltage in Figure 4(b). It is clear that the total ionization rate exhibits the same trend upon increasing dc voltage as the electron density (cf. Figure 3), i.e., it first increases, then decreases, and finally increases again with rising dc voltage. Hence, the ionization rate is directly responsible for the variation of electron density with dc bias.

For a deeper understanding of this behavior, we show the spatiotemporal ionization rates for different dc voltages in Figure 5. As illustrated in Figure 5(a), when the dc source is not applied, the maximum ionization rate appears during the phase of LF sheath collapse, which corresponds to the DF coupling effect.[29,30] Generally, the amplitude of the sheath oscillation depends on the local ion density, i.e., for a given sheath, if the ion density is low at the position of sheath oscillation, the corresponding amplitude of the sheath oscillation is large.[31] Due to flux continuity and the fact that

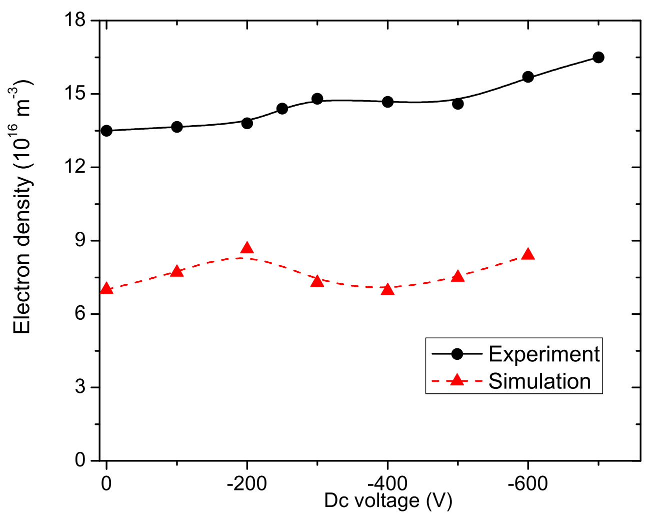

FIG. 3. Calculated (dashed line) and measured[11] (solid line) peak values of the electron density versus dc voltage. The experimental data were adopted with permission from T. Yamaguchi *et al.*, J. Phys. D: Appl. Phys. **45**, 025203 (2012). Copyright 2012 IOP publishing.

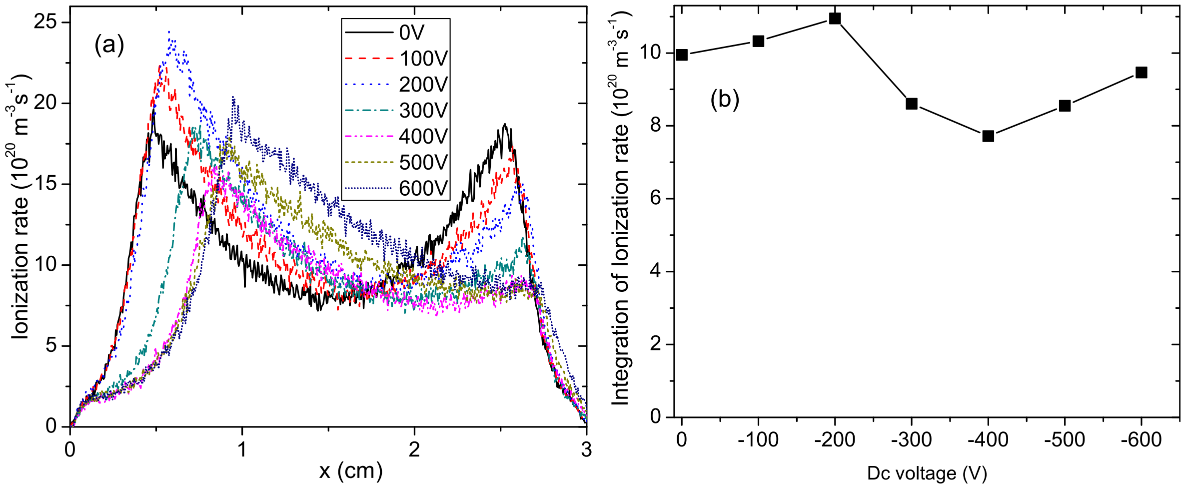

FIG. 4. (a) Calculated time-averaged ionization rate profiles for various dc voltages; (b) Spatially integrated values of the ionization rate as a function of dc voltage.

the ions are accelerated toward the electrode in the sheath, the ion density decreases monotonically from the plasma bulk toward the electrode in CCRF discharges. The ion density is thus very low in the thin LF sheath at the collapse phase, which results in a very large amplitude of HF sheath oscillations and consequently in very high ionization rates.

When applying a dc source of $-200\,\mathrm{V}$ to the bottom electrode, the behavior of the spatiotemporal distribution of the ionization rate is quite different within the two LF half-periods, as shown in Figure 5(b). The total voltage of dc and LF source is $V_{dc} + |V_{lf}\sin(2\pi f_{lf} t)|$ and $V_{dc} - |V_{lf}\sin(2\pi f_{lf} t)|$ in the two half-periods, respectively. In the first LF half-period, the negative dc bias is reduced to a certain extent by the LF source, especially during the phase of LF sheath collapse, when the LF voltage has the maximum value and the sheath becomes particular thin. In contrast, the net voltage on the bottom electrode becomes more negative than the applied dc bias in the second LF half-period, thus the plasma bulk, i.e., the corresponding volume where ionization occurs at low pressure, is greatly compressed and the ionization rate

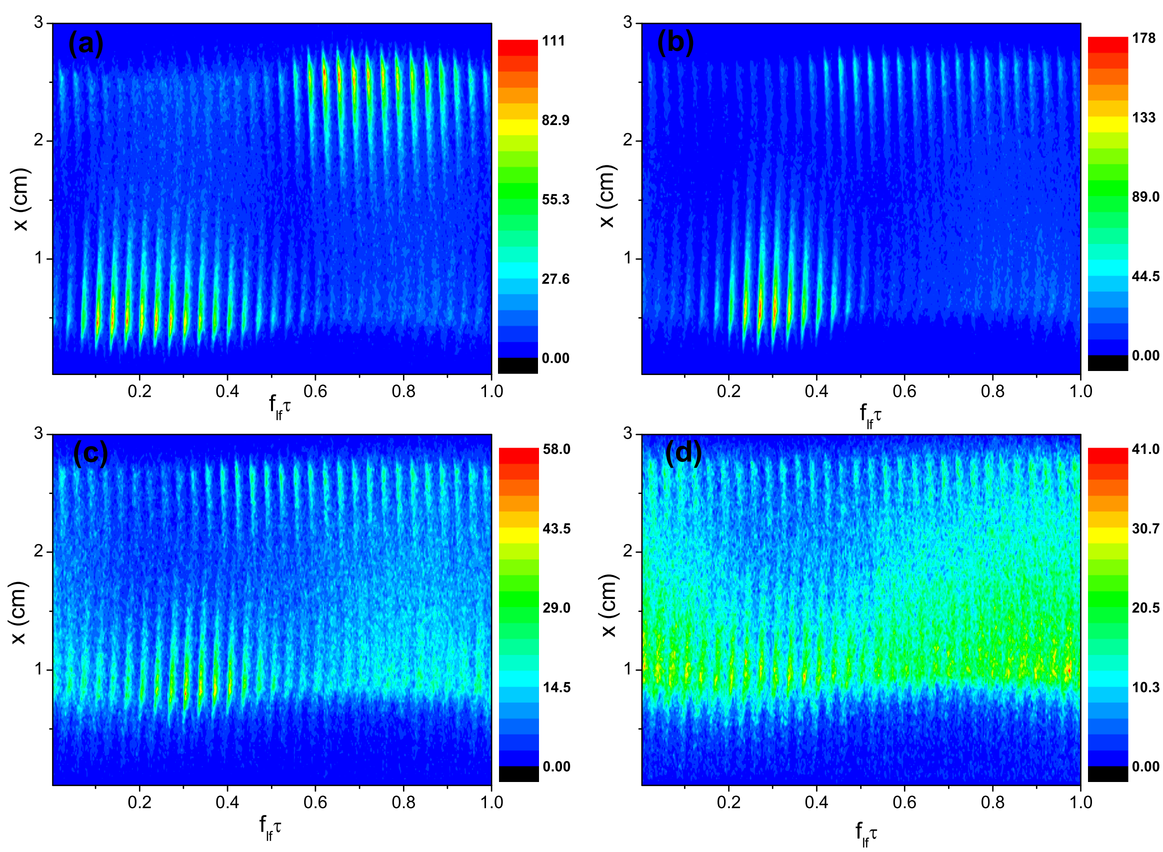

FIG. 5. Spatiotemporal distribution of the ionization rate (in units of $10^{20}\,\mathrm{m^{-3}s^{-1}}$) for one LF period with dc voltages of (a) 0 V, (b) -200 V, (c) -400 V, and (d)-600 V.

becomes very small. Besides, it should be noted that for most of the time of the LF period, the sheath close to the dc electrode is very large, and the plasma density in the sheath is extremely low (as shown in Figure 2(a)). Similar to the DF coupling effect above, this extremely low density causes a very large amplitude of HF sheath oscillations and very high ionization rates (almost twice the value without the dc source) around the phase of LF sheath collapse in the first LF half-period. Thus, the overall ionization rate and hence the plasma density increases, compared with the case without the dc source, as seen in Figures 4(b) and 3. We attribute this to the coupling of the dc and DF sources.

When further increasing the dc voltage to -400 V, the dc voltage cannot be reduced very much, because the amplitude of the LF source is only 250 V. Although the maximum ionization rate still appears around the phase of LF sheath collapse in the first LF half-period, the bulk plasma width is considerably reduced all over the LF period and the overall ionization drops, which leads to a decrease of the plasma density, as illustrated in Figures 4(b) and 3.

When further increasing the dc voltage to -600 V, the dc sheath becomes larger all over the LF period, and the ionization rate behaves quite differently from the previous cases. Indeed, more ionization appears in the bulk, around the phase of the large LF sheath, rather than at the edge of the sheath. This indicates that the plasma is maintained by secondary electron ionization instead of stochastic heating. Indeed, continuous ion bombardment on the dc electrode, because of the high dc voltage, induces an abundant flux of secondary electrons, which can be accelerated in the large dc/RF sheath to achieve high energy and give rise to a lot of ionization in the bulk. The discharge thus switches from the α mode to the γ mode,[26] even at this low pressure of 70 mTorr, which results in an increase of the plasma density again.

To summarize, the variation in electron density with rising dc voltage, as plotted in Figure 3, can be understood as follows: when a small dc voltage is applied (up to -200 V), two competitive effects in one LF period are observed. In the first LF half-period, the amplitude of the HF sheath oscillations and consequently the stochastic heating are enhanced upon increasing dc voltage. In the last LF half-period, the plasma bulk width is largely reduced and hence the Ohmic heating rate in the bulk drops. However, the overall ionization rate increases with rising dc voltage for the parameters studied here, which leads to an increase of the electron density, as seen in Figure 3. In this range of low applied dc voltages, the main heating mechanism is the coupling of the dc and DF sources.

When the dc voltage is larger than the amplitude of the LF source, the dc voltage cannot be compensated, completely, even at the phase when the LF voltage has the maximum value. The dc bias will dominate the discharge and the plasma bulk width is reduced over the entire LF period. Therefore, the overall ionization rate and hence the electron density decreases.

When further increasing the dc voltage, the secondary electrons gradually dominate the discharge. The discharge thus switches from the α mode to the γ mode[26] at high enough dc voltage, which results in an increase of the electron density again. The exact value of the dc voltage at which the electron density starts increasing again depends on the discharge pressure and material properties, more specifically, this value should be smaller at higher pressure or for electrode material with a larger secondary electron emission coefficient. Indeed, at high pressure, the secondary electrons will experience more collisions with neutral species, when going through the plasma bulk, hence contributing more to ionization. Similarly, there will be more secondary electrons emitted from a material with larger secondary electron emission coefficient. Both of these will promote the transition of the discharge from the α mode to the γ mode.

IV. CONCLUSION

We investigated the effect of electron heating in hybrid dc/DF CCRF discharges operated in CF_4 by means of 1D PIC/MCC simulations. The variation of plasma density with rising dc bias was compared with experimental data, and good qualitative agreement was reached. Four heating modes were observed in this hybrid dc/DF discharge: when no dc bias is applied, the discharge is mainly maintained by the DF coupling effect. When the dc voltage is comparable to the LF source amplitude, the coupling effect of dc and DF voltage becomes the main heating mechanism, and causes an increase of the plasma density. When the dc voltage is slightly larger than the LF source amplitude, the dc bias dominates the discharge and results in a compressed bulk region and hence a decrease of the plasma density. Finally, when the dc voltage becomes high enough, the high energy secondary electrons originating from the dc electrode contribute most to the ionization, which gives rise to an increase of the plasma density again.

ACKNOWLEDGMENTS

This work was supported by the National Natural Science Foundation of China (Grant No. 11335004), the Important National Science and Technology Specific Project (Grant No. 2011ZX02403-001), the International Science and Technology Cooperation Program of China (Grant No. 2012 DFG 02150), and the joint research project in the framework of the agreement between MOST and FWO-Flanders. Quan-Zhi Zhang gratefully acknowledges the Erasmus Mundus scholarship (EMEA scholarship programme). The calculations were performed using the Turing HPC infrastructure at the CalcUA core facility of the Universiteit Antwerpen, a division of the Flemish Supercomputer Center VSC, funded by the Hercules Foundation, the Flemish Government (department EWI), and the Universiteit Antwerpen.

[1]M. A. Lieberman and A. J. Lichtenberg, *Principles of Plasma Discharges and Materials Processing* (Wiley, New York, 2005).
[2]T. Makabe and Z. Petrović, *Plasma Electronics: Applications in Microelectronic Device Fabrication* (Taylor & Francis, Boca Raton, FL, 2006).
[3]H. H. Goto, H.-D. Lowe, and T. Ohmi, J. Vac. Sci. Technol. A **10**, 3048 (1992).

[4] T. Kitajima, Y. Takeo, Z. L. Petrovic, and T. Makabe, Appl. Phys. Lett. **77**, 489 (2000).
[5] G. Wakayama and K. Nanbu, IEEE Trans. Plasma Sci. **31**, 638 (2003).
[6] P. C. Boyle, A. R. Ellingboe, and M. M. Turner, Plasma Sources Sci. Technol. **13**, 493 (2004).
[7] M. M. Turner and P. Chabert, Phys. Rev. Lett. **96**, 205001 (2006).
[8] Z. Donko and Z. L. Petrovic, IOP Conf. Ser. **86**, 012011 (2007).
[9] Y. Lai, C. Hwang, A. Wang, R. Hwang, J. Yau, J. Liao, L. Chen, K. Adachi, and S. Okamoto, in *Proceedings of International Symposium on Dry Process* (Mentor Communications, 2006), Vol. 6, p. 109.
[10] T. Yamaguchi, T. Kimura, C. Koshimizu, K. Takeda, H. Kondo, K. Ishikawa, M. Sekine, and M. Hori, Jpn. J. Appl. Phys., Part 1 **50**, 056101 (2011).
[11] T. Yamaguchi, T. Komuro, C. Koshimizu, S. Takashima, K. Takeda, H. Kondo, K. Ishikawa, M. Sekine, and M. Hori, J. Phys. D: Appl. Phys. **45**, 025203 (2012).
[12] E. Kawamura, M. A. Lieberman, A. J. Lichtenberg, and E. A. Hudson, J. Vac. Sci. Technol. A **25**, 1456 (2007).
[13] E. Kawamura, A. J. Lichtenberg, and M. A. Lieberman, Plasma Sources Sci. Technol. **17**, 045002 (2008).
[14] W. Jiang, X. Xu, Z.-L. Dai, and Y.-N. Wang, Phys. Plasmas **15**, 033502 (2008).
[15] K. Denpoh and P. L. G. Ventzek, J. Vac. Sci. Technol. A **26**, 1415 (2008).
[16] P. L. G. Ventzek and K. Denpoh, J. Vac. Sci. Technol. A **27**, 287 (2009).
[17] L. Xu, L. Chen, M. Funk, A. Ranjan, M. Hummel, R. Bravenec, R. Sundararajan, D. J. Economou, and V. M. Donnelly, Appl. Phys. Lett. **93**, 261502 (2008).
[18] M. Wang and M. J. Kushner, J. Appl. Phys. **107**, 023308 (2010).
[19] M. Wang and M. J. Kushner, J. Appl. Phys. **107**, 023309 (2010).
[20] P. Diomede, S. Longo, D. J. Economou, and M. Capitelli, J. Phys. D: Appl. Phys. **45**, 175204 (2012).
[21] C. Birdsall and A. Langdon, *Plasma Physics via Computer Simulation* (McGraw-Hill, New York, 2004).
[22] J. Verboncoeur, M. Alves, V. Vahedi, and C. Birdsall, J. Comput. Phys. **104**, 321 (1993).
[23] J. P. Verboncoeur, Plasma Phys. Controlled Fusion **47**, A231 (2005).
[24] V. Georgieva, A. Bogaerts, and R. Gijbels, Phys. Rev. E **69**, 026406 (2004).
[25] M. M. Turner, Phys. Plasmas **13**, 033506 (2006).
[26] J. Schulze, Z. Donko, E. Schungel, and U. Czarnetzki, Plasma Sources Sci. Technol. **20**, 045007 (2011).
[27] K. Denpoh and K. Nanbu, Jpn. J. Appl. Phys., Part 1 **39**, 2804 (2000).
[28] O. V. Proshina, T. V. Rakhimova, A. T. Rakhimov, and D. G. Voloshin, Plasma Sources Sci. Technol. **19**, 065013 (2010).
[29] T. Gans, J. Schulze, D. O'Connell, U. Czarnetzki, R. Faulkner, A. R. Ellingboe, and M. M. Turner, Appl. Phys. Lett. **89**, 261502 (2006).
[30] M. M. Turner and P. Chabert, Plasma Sources Sci. Technol. **16**, 364 (2007).
[31] J. Schulze, Z. Donko, D. Luggenholscher, and U. Czarnetzki, Plasma Sources Sci. Technol. **18**, 034011 (2009).